Article

Novel Photocatalytic NH$_3$ Synthesis by NO$_3^-$ Reduction over CuAg/TiO$_2$

Ryota Kato [1],*, Mai Furukawa [1], Ikki Tateishi [2], Hideyuki Katsumata [1] and Satoshi Kaneco [1,2]

[1] Department of Chemistry for Materials, Graduate School of Engineering, Mie University, Mie 514-8507, Japan; maif@chem.mie-u.ac.jp (M.F.); hidek@chem.mie-u.ac.jp (H.K.); kaneco@chem.mie-u.ac.jp (S.K.)

[2] Global Environment Center for Education & Research, Mie University, Mie 514-8507, Japan; tateishi@gecer.mie-u.ac.jp

* Correspondence: rkato2.jpn@gmail.com; Tel.: +81-59-231-9427

Abstract: The highly effective reaction system was investigated for the photocatalytic ammonia synthesis from the reduction of nitrate ions by using the semiconductor photocatalyst, Cu and Ag doped on TiO$_2$ (CuAg/TiO$_2$) at room temperature under UV light irradiation (max. 352 nm). In this study, CuAg/TiO$_2$ gave the high efficiency and the selectivity for the ammonia synthesis by the photoreduction of nitrate in the presence of methanol as a hole scavenger. For the evaluation of the photocatalytic activity over CuAg/TiO$_2$, various TiO$_2$ samples, such as standard TiO$_2$, Cu/TiO$_2$, and Ag/TiO$_2$, were evaluated in the same procedure. The chemical properties were investigated by XRD, TEM, XPS, PL, and DRS. We examined the optimum conditions for the experimental factors and the important issues, including the effect of the molar ratio of Cu and Ag onto TiO$_2$, the optimization of the CuAg amount loaded on TiO$_2$, the influence of the loading amount of the catalyst on the reduction of nitrate ions, the exploration of the optimum hole scavenger, and the reusability of the optimum photocatalyst. The very efficient conversion of nitrate ions (95%) and the highest selectivity (86%) were achieved in the reaction with the optimum conditions. Here, we reported the process that nitrate ions can efficiently be reduced, and ammonia can be selectively synthesized over CuAg/TiO$_2$.

Keywords: ammonia synthesis; reduction of nitrate; photocatalyst; CuAg/TiO$_2$

1. Introduction

Ammonia (NH$_3$) has recently been recognized as one of the most important chemical products in the present world [1]. It is used for the chemical fertilizers, dyes, medicines, and so on. Also, it is expected to utilize the energy careers with the hydrogen production and substitute to the CO$_2$ free fuel [2]. Therefore, it clearly shows that the demand on the NH$_3$ production expands, as the population increases in the future. However, there are some serious problems in the present NH$_3$ production. In the current NH$_3$ synthesis, NH$_3$ is directly synthesized by N$_2$ and H$_2$ over an iron-based catalyst (Haber-Bosch process). However, this method needs the conditions at high temperature (400–500 °C) and high pressure (150–250 bar), which is not a sustainable process in the NH$_3$ production for a long time. In addition to this disadvantage, a large amount of fossil fuels is consumed, and its production simultaneously releases a huge amount of CO$_2$ [3]. Therefore, these issues may create significantly negative effects for the environment on the earth. Many studies were evaluated for the NH$_3$ synthesis with the operation using the low energy without using fossil fuel [4]. As the method for the substitution of Haber Bosch process, various ammonia production processes were investigated such as following methods; the plasma catalysis [5], the electrochemical system [6], the production from biomass [7].

The nitrate ion (NO$_3^-$) reduction by using the photocatalysts should be noted as the method to synthesize NH$_3$. Various photocatalysts were applied into the new approaches for the photocatalytic

NH_3 synthesis are as follows: M/TiO_2 (M = Ru, Rh, Pd, Pt) [8], Ru/C [9], $Au/SrTiO_3$ [10], and BiOCl [11] as the photocatalysts for synthesizing NH_3 at a lower reaction temperature and pressure. For the application to the industrial process, it is suggested that NO_3^- is separated from wastewater by the ion exchange method, and the catalyst is added to this treated water including NO_3^-. After the photocatalytic reduction of NO_3^- in the treated water, ammonium ions are generated in the solution. This can be collected as ammonia by the ammonia stripping process. In this process, ammonia is released in the gas phase by adjusting to the basic pH condition. However, the above catalysts did not indicate the high reactivity in the reduction processes because of the poor photocatalytic activity.

Titanium dioxide (TiO_2) is one of the well-known semiconductor photocatalysts, which absorb the UV light and can cause the photocatalytic reaction. Also, TiO_2 has some advantages such as the very high stability in the solution with the various pH, the low cost, and the high practicality due to easy handling [12]. Therefore, the reaction system of the photocatalytic NO_3^- reduction to NH_3 over metal-doped TiO_2 may be significant as a green process for the photocatalytic NH_3 synthesis by the reduction of NO_3^- in the lower energy without using fossil fuel. As the source of N_2, NO_3^- has attracted attention by the recent studies because it is the very toxic pollutant in the waste water and gives the very harmful effect to human health [13]. Therefore, the NH_3 synthesis by using NO_3^- as a raw material may enable to contribute to the improvement of the environmental issues by the decontamination of waste water including NO_3^- and the development of the excellent ecological approach for the NH_3 production.

However, the reduction efficiency of NO_3^- and the selectivity of NH_3 are still very poor in the photocatalytic reduction of NO_3^- [14]. Methanol (CH_3OH) may be applied into the reduction of NO_3^- to improve this problem. Generally, CH_3OH was used as a hole scavenger and it was oxidized to formaldehyde by holes. Also, the reduction simultaneously produces reactive hydrogen [15], which results in the more efficient reduction of NO_3^-. Thus, CH_3OH may become very useful for the photocatalytic NO_3^- reduction.

In the present study, we used Cu and Ag as doping metals for the preparation of photocatalysts. Cu is one of the well-known metals and it is widely applied to the photocatalysts because it has several advantages of the high electro conductivity and the low cost. Noble metals, such as Au, Ag, and Pt show the localized surface plasmonic resonance (LSPR), which has the ability to absorb the visible light [16]. It can improve the photoabsorption by its light trapping effects [17]. Also, it is indicated that these metals nanoparticles can perform as an electron donor to promote the electron transfer from metal to semiconductor [18,19]. In addition to this function, these metals can suppress the recombination of surface electrons and holes [20,21]. In the photocatalytic reaction over these metals doped TiO_2, Kamat et al. proposed that the excited electrons were transferred in these metals to TiO_2. Therefore, the Cu and Ag doped TiO_2 photocatalyst minimized the recombination of photoelectron-hole and gave the high photoabsorption and the proper bandgap for the photocatalytic reaction [22]. Here, we investigated the method for the selective NH_3 synthesis by the photocatalytic reduction of NO_3^- over Cu and Ag doped TiO_2 ($CuAg/TiO_2$). The reaction was operated in the presence of 50 ppm of NO_3^- aqueous solution including 10 vol% CH_3OH at room temperature under UV irradiation (λ: max. 352 nm). In the present work, we examined in detail the photocatalytic activity, the optimization of the experimental conditions, and the reusability of the optimum catalyst. This reaction system would give the excellent approach for the selective NH_3 synthesis by photocatalytic NO_3^- reduction over the optimized photocatalyst.

2. Materials and Methods

2.1. Materials

Titanium dioxide (TiO_2-P25, 99.50%) was purchased from Degussa Co. Cu 1000 ppm standard solution $Cu(NO_3)_2$ in 0.1 mol/L HNO_3 was obtained from FUJIFILM Wako Pure Chemical Corp. Ag 1000 ppm standard solution ($AgNO_3$ in 0.1 mol/L HNO_3) and potassium nitrate (KNO_3) were

obtained from Nacalai Tesque Inc. All of the reagents and the materials used in this research were analytical grade and were used without further purification. KNO_3 and distilled water were used for the preparation of the simulated waste water including NO_3^-. Methanol (CH_3OH) was added to the simulated waste water as a hole scavenger. For the evaluation of the optimum hole scavenger, ethanol (C_2H_5OH), isopropyl alcohol ((CH_3)$_2$CHOH), and *t*-butyl alcohol ((CH_3)$_3$COH) were applied in this study.

2.2. Preparation of TiO$_2$ Samples

Cu^{2+} 1000 ppm standard solution, Ag^+ 1000 ppm standard solution and 300 mg of TiO_2 were added in 10 vol% CH_3OH aqueous solution. The total amount of metals (Cu and Ag) were 1 wt% for the amount of TiO_2. The mixed solution was stirred under blacklight irradiation (λ: max 352 nm) for an hour. After the centrifugation, the supernatant was removed, and the photocatalyst was dried under vacuum overnight. The different TiO_2 samples were obtained in this preparation method (Table S1). The obtained products were used for NH_3 synthesis by NO_3^- reduction.

2.3. Characterization

X-ray diffraction (XRD) was performed by Ultima IV, RIGAKU with Cu-Kα radiation, equipped with the graphite monochromator on the diffracted beam. The morphology of the catalysts was operated by transmission electron microscope (TEM) using JEM-1011, HITACHI. X-ray photoelectron spectroscopy (XPS) was measured by PHI Quantera SXM, ULVAC-PHI. The C1s peak at 284.6 eV was used to calibrate all of the binding energy. The photoluminescence spectra (PL) were given by a fluorescence spectrophotometer (RF-5300PC, SHIMADZU) at an excitation wavelength of 330 nm using D_2 lamp at ambient temperature. UV-Vis diffuse reflectance spectra (DRS) were operated on V-750 spectrophotometer, JASCO in the range of 200–800 nm using D_2 lamp.

2.4. Photocatalytic Reduction of NO$_3^-$ to NH$_3$

The photocatalytic reduction of NO_3^- was performed in the Pyrex reactor. Firstly, 50 ppm of NO_3^- aqueous solution (45 mL) including 10 vol% CH_3OH was prepared, and 30 mg of the photocatalyst was added to the solution. The suspension was stirred with a magnetic stirrer at room temperature under UV irradiation for 3 hours. As the light source, black light (max: 352 nm) was used for NO_3^- reduction. The measurements of the concentration of ions (NO_3^-, NO_2^-, and NH_4^+) in the solution after the reaction were performed by ion chromatography (Metrohm Compact IC 761).

3. Results and Discussion

3.1. Calculation of the NO$_3^-$ Conversion and Selectivity

The NO_3^- conversion and the selectivity of the products were calculated by the following equations:

$$C_{NO_3^-} = \frac{\left[n_{NO_3^-}\right]_0 - \left[n_{NO_3^-}\right]_t}{\left[n_{NO_3^-}\right]_0} \tag{1}$$

$$S_{NO_2^-} = \frac{\left[n_{NO_2^-}\right]_t}{\left[n_{NO_3^-}\right]_0 - \left[n_{NO_3^-}\right]_t} \tag{2}$$

$$S_{NH_4^+} = \frac{\left[n_{NH_4^+}\right]_t}{\left[n_{NO_3^-}\right]_0 - \left[n_{NO_3^-}\right]_t} \tag{3}$$

$$S_{N_2 \text{ product}} = 100 - \left(S_{NO_2^-} + S_{NH_4^+}\right) \tag{4}$$

where $[n]_0$ is the amount of material (mmol) at time = 0 and $[n]_t$ is the amount of material (mmol) at time = t.

3.2. Characterization of Photocatalysts

X-ray diffraction (XRD) spectra of various TiO_2 samples were shown in Figure 1. The TiO_2 P25 particle is consisted of anatase phase and rutile phase. The structure ratio of anatase phase and rutile phase are 80% and 20%, respectively. The characteristic patterns of anatase phase were clearly found at 2θ = 25.2° (101), 37.0° (103), 37.9° (200), 48.0° (200), 53.9° (105), 55.0° (211), 62.8° (204), and 75.1° (215). The typical patterns of the rutile phase were observed at 2θ = 27.5° (110), 36.0° (101), 41.3° (111), 56.5° (220), 62.0° (002), 64.2° (311), 69.0° (301), and 70.3° (112) [23]. These sharp peaks showed that the crystallinity of all TiO_2 samples was very high. However, the peaks of Cu and Ag were not confirmed due to the relatively low amount of metals loaded on TiO_2. Also, the XRD results of other TiO_2 samples used in this study were summarized in Figure S1.
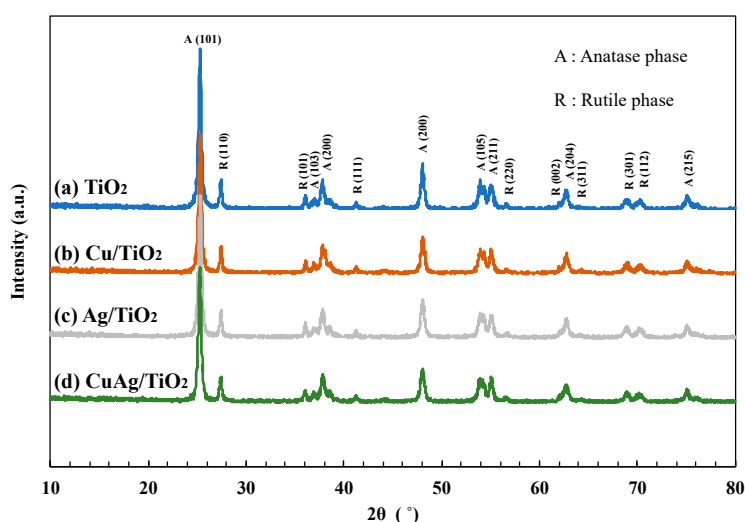
**Figure 1.** XRD spectra of (**a**) TiO_2 P25, (**b**) Cu/TiO_2, (**c**) Ag/TiO_2 and (**d**) $CuAg/TiO_2$.

The TEM images of the photocatalysts were shown in Figure 2. As a result, the existence of Cu and Ag was not confirmed, as the amount of Cu and Ag was very low compared with the amount of TiO_2. On the other hand, it was obviously confirmed that all of the TiO_2 samples had the same morphology. Therefore, it was indicated that the morphology of photocatalyst could not be changed by doping Cu and Ag. TEM images of other TiO_2 samples used in this study were shown in Figure S2. All of the TiO_2 samples were nanoparticles and the size were roughly 20–30 nm. Cu and Ag particles were not observed because they are too small to be detected by TEM.

For the identification of the composition of Cu and Ag on TiO_2, X-ray photoelectron spectroscopy (XPS) was applied to the $Cu_{0.9}Ag/TiO_2$ composite photocatalyst (Figure 3). The peak of C1s was used for the calibration, which was attributed to the contaminated carbon [24,25].

In the O 1s signals, the presence of Ti-O of titania at about 530 eV could be confirmed, and the peak at 528.9 eV was attributed to CO (Figure 3a) [26]. The spectrum region corresponding to Ti 2p revealed that two peaks at 464.1 eV and 458.6 eV were due to Ti $2p_{1/2}$ and Ti $2p_{3/2}$, respectively. As the results, we assigned it with 4+ oxidation number by analyzing the intensity of Ti $2p_{3/2}$ of this sample. These peaks were highly sharp and intense, so that it indicated that this photocatalyst consists only of Ti^{4+} species [27]. This result shows that $Cu_{0.9}Ag/TiO_2$ was properly prepared and its structure was not changed by the deposition of Cu and Ag under UV irradiation.
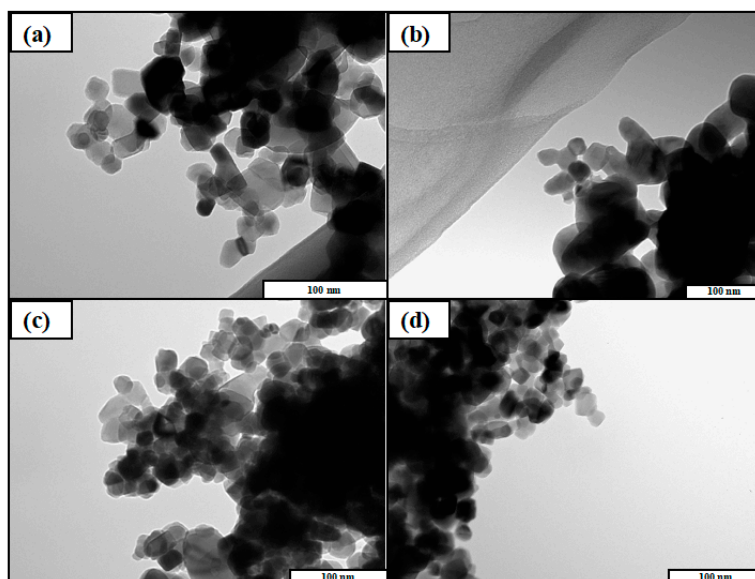
Figure 2. Transmission electron microscope (TEM) images of (**a**) TiO_2, (**b**) Cu/TiO_2, (**c**) Ag/TiO_2, and (**d**) $Cu_{0.9}Ag/TiO_2$.

The narrow scan of Cu 2p of $Cu_{0.9}Ag/TiO_2$ showed two peaks at 950.9 eV and 931.9 eV and these peaks were attributed to Cu $2p_{1/2}$ and Cu $2p_{3/2}$, respectively (Figure 3c). However, it cannot easily be distinguished between Cu^0 and Cu^{2+}, because the difference of the binding energy between Cu^0 and Cu^{2+} is only 0.1 eV. In addition, Ag 3d peaks at 373.2 eV and 367.1 eV were corresponding to Ag $3d_{3/2}$ and Ag $3d_{5/2}$, respectively (Figure 3d) [28]. These characteristic peaks indicated that it was existed as metal Ag [29].

As a result, the existence of Cu and Ag was confirmed in the samples, and all of elements including O, Ti, Cu, and Ag were observed. It clearly showed that Cu and Ag were successfully formed on TiO_2. In addition to these results, XPS spectra of other TiO_2 samples used in this study were shown in Figures S3–S6.
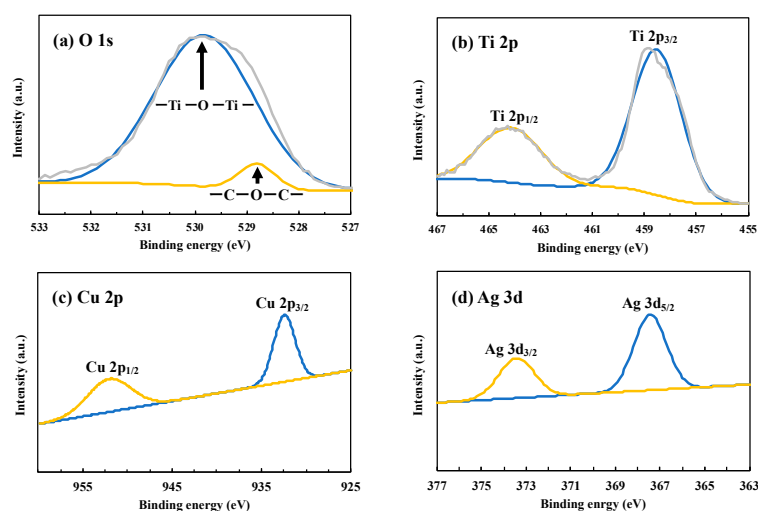
Figure 3. XPS spectra of (**a**) O 1s, (**b**) Ti 2p, (**c**) Cu 2p, and (**d**) Ag 3d over $CuAg/TiO_2$.

UV-Vis diffuse reflectance spectra (DRS) were evaluated to identify the optical absorption properties (Figure 4). The absorption edge of the standard TiO_2 was about 380 nm. All of TiO_2 samples were confirmed to show the light absorption in the UV region, and the intensity was enhanced by

loading Cu and Ag doped on TiO_2. In this research, the band-gap energy was calculated by following formula [30]:

$$E_g \text{ (eV)} = 1240/\lambda_g \text{ (nm)} \tag{5}$$

where E_g refers to the band-gap energy and λ_g is the wavelength at the absorption edge [16]. The band-gap energies E_g of TiO_2 and $Cu_{0.9}Ag/TiO_2$ were estimated to 3.26 eV and 2.92 eV, respectively.
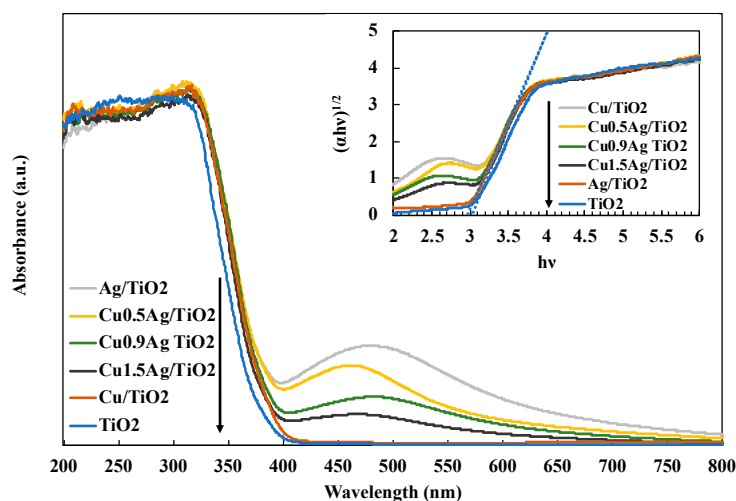

Figure 4. DRS spectra of various TiO_2 samples.

Photoluminescence (PL) spectra were measured to examine the recombination of electron-hole over the photocatalysts (Figure 5). All of the PL spectra were obtained in the range of 350–600 with an excitation wavelength at 330 nm. The comparison of TiO_2 and metals-doped TiO_2 samples was investigated in Figure 5a. Compared with standard TiO_2, metal-doped TiO_2 samples showed the low intensity. It revealed that loading metals gave the decrease of the PL intensity, and the recombination of photogenerated electron and hole was suppressed by doping metals on TiO_2. This reason may be considered it that the electrons were efficiently trapped by CuAg bimetal. The PL spectra of the TiO_2 samples with the different amount of the CuAg doped on TiO_2 were shown in Figure 5b. As the amount of CuAg increased, the PL intensity decreased. Therefore, the doping of Cu and Ag gave the good effect on the recombination of charge careers, which showed the high photocatalytic activity.
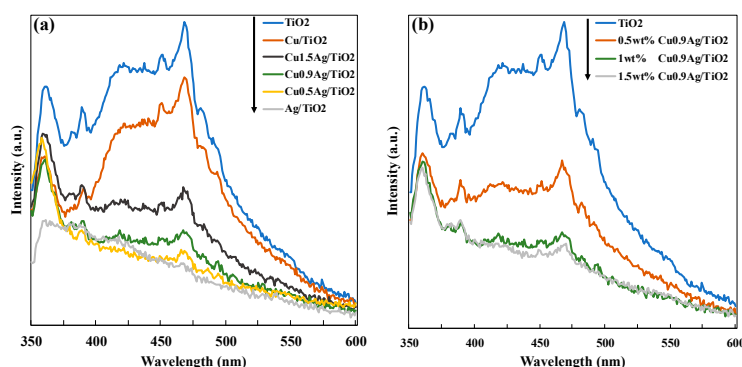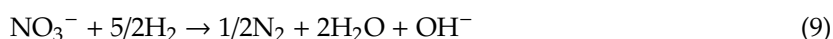

Figure 5. (**a**) Comparison of PL spectra of the different TiO_2 samples, and (**b**) effect of the loading amount of CuAg alloy onto TiO_2.

3.3. Photocatalytic Activity in NO_3^- Reduction to NH_3

Firstly, the evaluation for the photocatalytic activity in the reduction of NO_3^- to NH_3 was performed over TiO_2 alone, Cu/TiO_2, Ag/TiO_2, and $CuAg/TiO_2$ in the presence of CH_3OH under UV irradiation for three hours (Figure 6). The amount of photocatalyst was 30 mg in all of test cases. In the

photocatalytic NO_3^- reduction, NH_4^+, NO_2^-, and N_2 seem to be mainly generated as the products. In addition, CH_3OH was oxidized to $HCHO$ by a photocatalytic reaction as a hole scavenger and the reduction produced hydrogen, which played an important role in NO_3^- reduction by following the equations:

$$2H^+ + 2e^- \rightarrow H_2 \tag{6}$$

$$NO_3^- + H_2 \rightarrow NO_2^- + H_2O \tag{7}$$

$$NO_3^- + 4H_2 \rightarrow NH_4^+ + H_2O + 2OH^- \tag{8}$$

$$NO_3^- + 5/2H_2 \rightarrow 1/2N_2 + 2H_2O + OH^- \tag{9}$$

As a result, $Cu_{0.9}Ag/TiO_2$ gave the very efficient NO_3^- conversion (96%) and the highest NH_3 selectivity (85%), while the NO_3^- conversion and the NH_3 selectivity over TiO_2 alone were only 44.9% and 33.6%, respectively. Also, the reaction had not occurred without the photocatalyst. In addition to these results, the comparison of the photocatalytic activity with other catalysts was performed (Table S2). Consequently, it clearly showed that loading the optimum amount of Cu and Ag onto TiO_2 gave the excellent photocatalytic activity in the reduction of NO_3^- to NH_3. Hence, $CuAg/TiO_2$ was very useful to photocatalytic NO_3^- reduction rather than other TiO_2 samples.
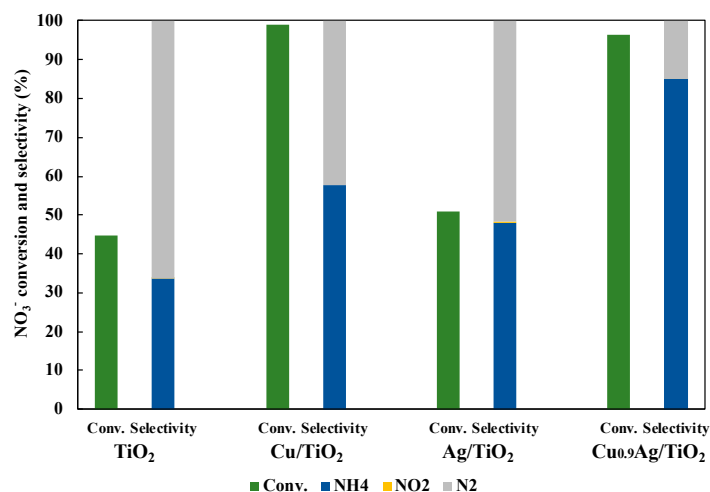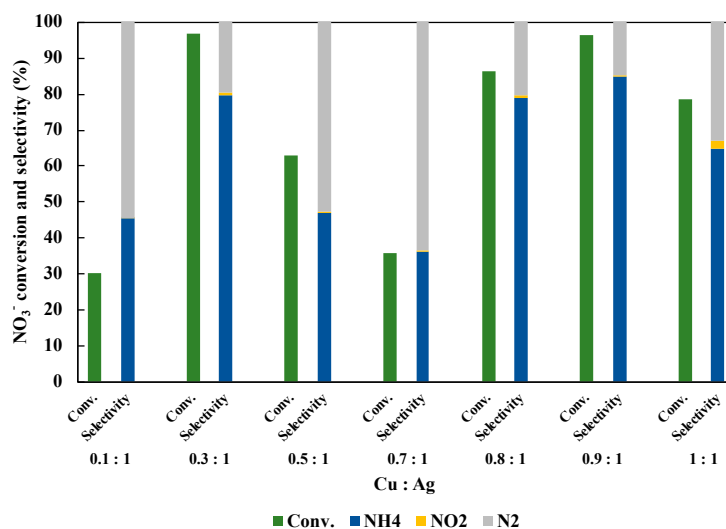

Figure 6. Comparison of photocatalytic activity over TiO_2, Cu/TiO_2, Ag/TiO_2 and $Cu_{0.9}Ag/TiO_2$ in 45 mL of 50 ppm NO_3^- aqueous solution including 10 vol% CH_3OH under UV irradiation for three hours. The loading amount of each samples was 30 mg. Left bar is NO_3^- conversion, right bars (blue, yellow, and gray) are product selectivity (NH_4^+, NO_2^-, and N_2 product, respectively).

3.4. Optimization of Structure and Loading Amount of CuAg/TiO2

We optimized the molar ratio of Cu and Ag doped on TiO_2 (Figure 7). The total amount of Cu and Ag was controlled to be 1 wt% of TiO_2 amount. As shown in the result, the highest NO_3^- conversion and the NH_3 selectivity were achieved over $Cu_{0.9}Ag/TiO_2$ (Cu:Ag = 0.9:1). Consequently, both the NO_3^- conversion and NH_4^+ selectivity was respectively almost same when $Cu_{0.3}Ag/TiO_2$ and $Cu_{0.9}Ag/TiO_2$ were used. Silver is one of the precious metals and it is so expensive for the application to the chemical industry. This means that the catalyst with the lower Ag amount (Cu:Ag = 0.9:1) is better than the catalyst with higher Ag amount (Cu:Ag = 0.3:1). Therefore, we selected Cu:Ag = 0.9:1 as an optimum molar ratio in this study.

Figure 7. Effect of molar ratio of Cu and Ag loaded on TiO$_2$ in 45 mL of 50 ppm NO$_3^-$ aqueous solution including 10 vol% CH$_3$OH under UV irradiation for three hours. The loading amount of each samples was 30 mg.

In addition to the optimization of the molar ratio, the loading amount of Cu$_{0.9}$Ag on TiO$_2$ was investigated (Figure 8). The NO$_3^-$ conversion and the NH$_3$ selectivity were improved as the loading amount of Cu$_{0.9}$Ag increased. When the excess amount of the catalyst was used, the photocatalytic activity decreased. The highest NO$_3^-$ conversion and the NH$_3$ selectivity were given by 1 wt% of Cu$_{0.9}$Ag doped on TiO$_2$. Therefore, 1 wt% Cu$_{0.9}$Ag/TiO$_2$ was used as an optimum photocatalyst in this study.
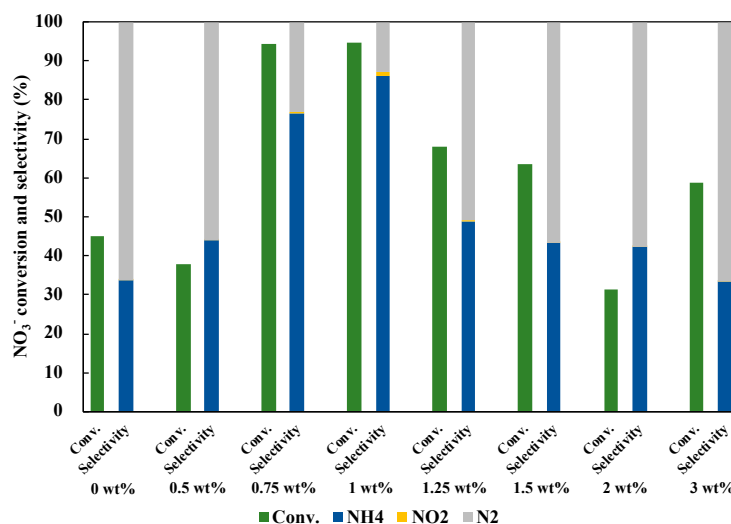
Figure 8. Effect of loading amount of Cu$_{0.9}$Ag on TiO$_2$ in 45 mL of 50 ppm NO$_3^-$ aqueous solution including 10 vol% CH$_3$OH under UV irradiation for three hours. The loading amount of each samples was 30 mg.

After the optimization to the structure of the photocatalyst, we investigated the optimum dosage of the photocatalyst in the reduction of NO$_3^-$ to NH$_3$ over 1 wt% Cu$_{0.9}$AgTiO$_2$ (Figure 9). This experiment was performed in the presence of CH$_3$OH under UV irradiation for nine hours, and the photocatalysts in the range of 10–40 mg were used. Loading 30 mg and 40 mg of the catalyst gave the significantly high NO$_3^-$ reduction rate (Figure S7). Thus, we selected 30 mg as an optimum dosage of the photocatalyst in the NO$_3^-$ reduction, because it can perform the reduction of NO$_3^-$ with the lower catalyst amount. In this study, we fixed 30 mg of 1 wt% Cu$_{0.9}$Ag/TiO$_2$ as the optimal conditions for the reaction system.
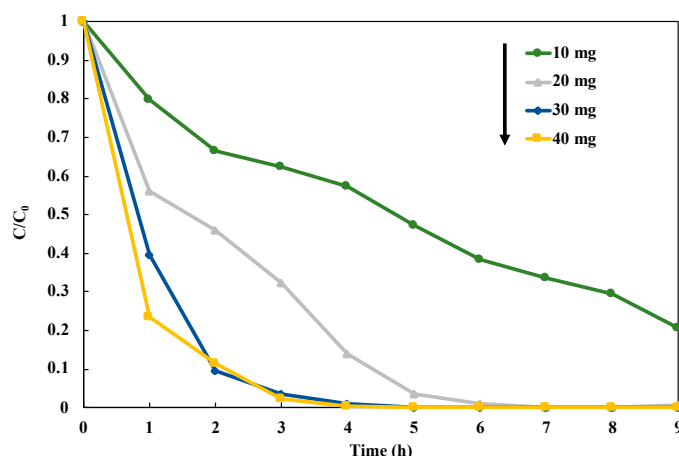
Figure 9. Influence of loading catalyst amount on NO_3^- reduction in 45 mL of 50 ppm NO_3^- aqueous solution including 10 vol% CH_3OH under UV irradiation for nine hours.

3.5. Effect of Hole Scavenger on NO_3^- Reduction to NH_3

The hole scavenger was also the very important factor in the reaction with the photocatalyst. Figure 10 shows the effect of the hole scavenger on the reduction of NO_3^- to NH_3. As a result, CH_3OH indicated the most efficient NO_3^- conversion and the NH_3 selectivity. In the photocatalytic NO_3^- reduction, CH_3OH was turned to HCHO with h^+, and then H_2 was simultaneously released. Generated H_2 on the photocatalyst surface was useful to reduce NO_3^- and NO_2^- (Equations (6)–(11)).

$$NO_2^- + 3H_2 \rightarrow NH_4^+ + 2OH^- \tag{10}$$

$$2NO_2^- + 2H_2 \rightarrow N_2 + 4OH^- \tag{11}$$

On the other hand, it is considered that C_2H_5OH, $(CH_3)_2CHOH$, and $(CH_3)_3COH$ were not so reactive, because of the larger steric hindrance. Therefore, CH_3OH could give more H_2 than those with other hole scavengers, and CH_3OH was selected as an optimal hole scavenger in this study.
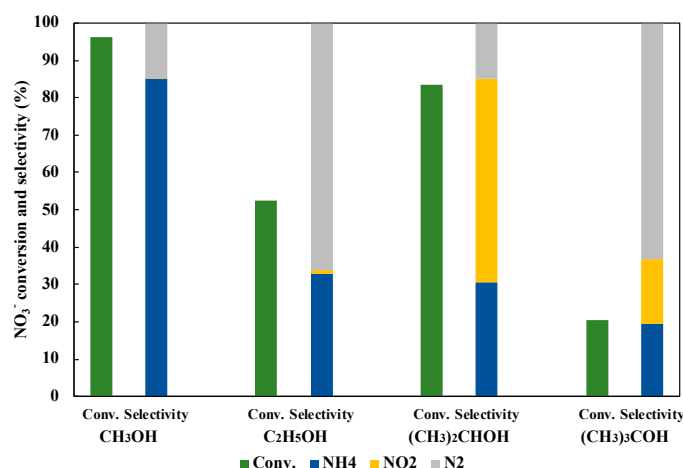

Figure 10. Effect of hole scavengers on NO_3^- reduction to NH_3 in 45 mL of 50 ppm NO_3^- aqueous solution including 10 vol% of hole scavenger under UV irradiation for three hours.

3.6. Effect of pH

We checked the pH effect in the solution during the NO_3^- reduction under UV irradiation for three hours (Figure 11). The initial pH value was about six without the pH adjustment. The NO_3^- conversion and the selectivity of NH_3 decreased under pH = 5. This reason may be owing to it that the

protons in the solution were not sufficiently reacted with NO_3^- adsorbed on the catalyst surface, as the protons repelled to the positive charges on the photocatalyst surface. Under alkaline conditions, the NO_3^- conversion was kept high, while the NH_3 selectivity decreased compared with the case of pH = 6. There are two proposed reasons; i) some •OH radicals were generated in the solution, which promoted the oxidation of methanol. Hence, the reduction rate of NO_3^- was simultaneously enhanced and more NO_2^- ions and N_2 products were generated; ii) the H^+ concentration in the solution decreased under alkaline conditions, which leads to inhibit further reductions of NO_2^- to NH_4^+. On the other hand, the high NO_3^- conversion and the NH_3 selectivity were achieved without the pH adjustment (pH = 6). This result may be shown that it was given by the sufficiently high H^+ concentration and the good adsorption of NO_3^- on the catalyst surface under pH = 6.
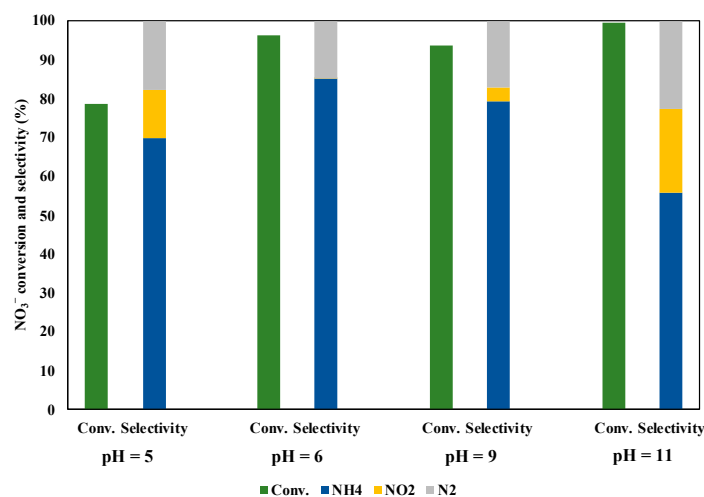
Figure 11. pH effect in solution during NO_3^- reduction under UV irradiation for three hours.

3.7. Reusability of Photocatalyst in NO_3^- Reduction to NH_3

We investigated the reusability of 1 wt% $Cu_{0.9}Ag/TiO_2$ photocatalyst in the reduction of NO_3^- to NH_3 under UV irradiation for three hours. Five repeated experiments were operated to evaluate the stability of the optimum photocatalyst. As shown in Figure 12, the NO_3^- conversion and the NH_3 selectivity were changed for each cycle. It may be owing to the loss of the catalyst amount in the operation for sample collection. Therefore, it is considered that the photocatalytic activity was not degraded by five cycles. It clearly shows that the stability of 1 wt% $Cu_{0.9}Ag/TiO_2$ in this research.
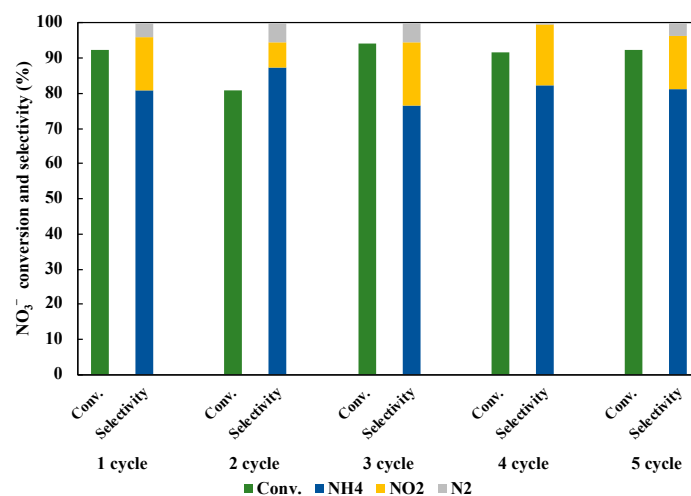
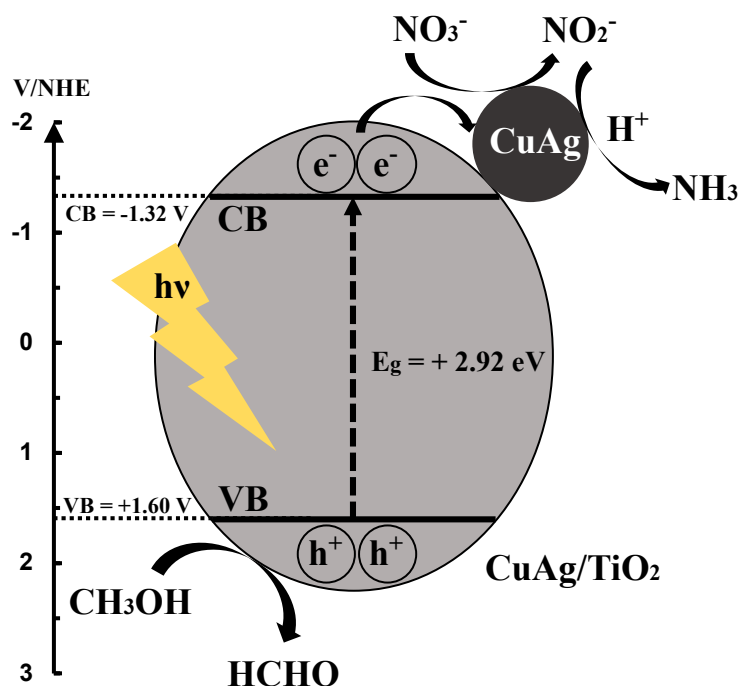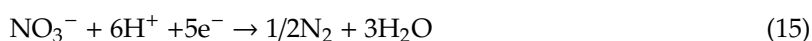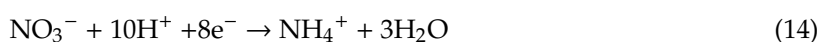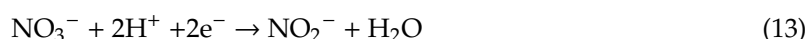**Figure 12.** Reusability of 1 wt% $Cu_{0.9}Ag/TiO_2$ in 45 mL of 50 ppm NO_3^- aqueous solution including 10 vol% of CH_3OH under UV irradiation for three hours for five cycles.

3.8. Reaction Mechanism of Photocatalytic NO_3^- Reduction to NH_3

Scheme 1 shows the proposed reaction mechanism of $CuAg/TiO_2$ in this study. First, $CuAg/TiO_2$ is stimulated by UV light, and electrons and holes are generated. The photogenerated electrons in conduction band are transferred to valence band, and then are moved to CuAg alloy. NO_3^- is reduced to NO_2^- with the electrons, and NO_2^- is reduced to NH_3 with the electrons and protons. The hole scavenger, CH_3OH is oxidized to $HCOOH$ with holes, and H_2 was released, which gives further reduction of NO_3^-. The oxidation of methanol to formaldehyde was confirmed by the experiment shown in Figure S7.

The reaction processes can be expressed as following formulas:

$$\text{Photocatalyst} \overset{h\nu, \text{cat.}}{\rightarrow} h^+ + e^- \tag{12}$$

$$NO_3^- + 2H^+ + 2e^- \rightarrow NO_2^- + H_2O \tag{13}$$

$$NO_3^- + 10H^+ + 8e^- \rightarrow NH_4^+ + 3H_2O \tag{14}$$

$$NO_3^- + 6H^+ + 5e^- \rightarrow 1/2N_2 + 3H_2O \tag{15}$$

Scheme 1. Reaction mechanism of $CuAg/TiO_2$ in NO_3^- reduction to NH_3.

4. Conclusions

The significantly effective photocatalyst $CuAg/TiO_2$ was prepared for the highly selective NH_3 synthesis by photocatalytic reduction of NO_3^-. Cu to Ag molar ratio of 0.9:1 and 1 wt% $Cu_{0.9}Ag$ doped TiO_2 indicated the excellent NO_3^- conversion and the NH_3 selectivity. These results were brought by the advantages of the CuAg alloy and the presence of CH_3OH in the reduction of NO_3^-. Loading Cu and Ag onto TiO_2 gave the effective separation of electron-hole pairs and enhanced the light absorption in UV region. CH_3OH was used as the optimum hole scavenger for the source of H_2. From the result of the cycle test, the stability of $CuAg/TiO_2$ was indicated by five cycles.

images of (a) TiO_2, (b) Cu/TiO_2, (c) Ag/TiO_2, (d) $Cu_{0.5}Ag/TiO_2$, (e) $Cu_{0.9}Ag/TiO_2$, (f) $Cu_{1.5}Ag/TiO_2$, (g) 0.5 wt% $Cu_{0.9}Ag/TiO_2$, and (h) 1.5 wt% $Cu_{0.9}Ag/TiO_2$, Figure S3: O 1s core level spectra in TiO_2 samples, Figure S4: Ti 2p core level spectra in TiO_2 samples, Figure S5: Cu 2p core level spectra in TiO_2 samples, Figure S6: Ag 3d core level spectra in TiO_2 samples, and Figure S7: Oxidation of methanol to HCOOH during NO_3^- reduction under UV irradiation for 3 h.

Author Contributions: R.K. and S.K. conceived and designed the experiments. R.K. performed the experiments and wrote the paper. I.T., M.F. and H.K. analyzed the results and advised the project.

Conflicts of Interest: The authors declare no conflict of interest.

References

1. Gruber, N.; Galloway, J.N. An earth-system perspective of the global nitrogen cycle. *Nature* **2008**, *451*, 293–296. [CrossRef] [PubMed]
2. Giddey, S.; Badwal, S.P.S.; Kulkarni, A. Review of electrochemical ammonia production technologies and materials. *Int. J. Hydrogen Energy* **2013**, *38*, 14576–14594. [CrossRef]
3. McEaney, J.M.; Singh, A.R.; Schwalbe, J.A.; Kibsgaard, J.; Lin, J.C.; Cargnello, M.; Jaramillo, T.F.; Nørscov, J.K. Ammonia synthesis from N_2 and H_2O using a lithium cycling electrification strategy at atmospheric pressure. *Energy Environ. Sci.* **2017**, *10*, 1621–1630. [CrossRef]
4. Baltrusaitis, J. Sustainable ammonia production. *ACS Sustain. Chem. Eng.* **2017**, *5*, 9527. [CrossRef]
5. Jungmi, H.; Steven, P.; Anthony, B.M. Plasma catalysis as an alternative route for ammonia production: status, mechanisms, and prospects for progress. *ACS Sustain. Chem. Eng.* **2018**, *6*, 15–31.
6. Yusuf, B.; Ibrahim, D. Assessment of a sustainable electrochemical ammonia production system using photoelectrochemically produced hydrogen under concentrated sunlight. *ACS Sustain. Chem. Eng.* **2017**, *5*, 8035–8043.
7. Pratham, A.; Andrew, F.A.H.; Sanjay, M.M.; Anuradda, G. Small-scale ammonia production from biomass: A techno-enviro-economic perspective. *Ind. Eng. Chem. Res.* **2016**, *55*, 6422–6434.
8. Ranjit, K.T.; Varadarajan, T.K.; Viswanathan, B. Photocatalytic reduction of dinitrogen to ammonia over noble-metal-loaded TiO_2. *J. Photochem. Photobiol. A Chem.* **1996**, *96*, 181–185. [CrossRef]
9. Ozaki, A.; Aika, K. Catalytic activation of dinitrogen. *Catal. Sci. Technol.* **1981**, *1*, 87–158.
10. Oshikiri, T.; Ueno, K.; Misawa, H. Plasmon-induced ammonia synthesis through nitrogen photofixation with visible light irradiation. *Angew. Chem. Int. Ed. Engl.* **2014**, *53*, 9802–9805. [CrossRef] [PubMed]
11. Li, H.; Shang, J.; Shi, J.; Zhao, K.; Zhang, L. Facet-dependent solar ammonia synthesis of BiOCl nanosheets via a proton-assisted electron transfer pathway. *Nanoscale* **2016**, *8*, 1986–1993. [CrossRef] [PubMed]
12. Koltsakidou, A.; Antonopoulou, M.; Evgenidou, E.; Konstantinou, I.; Gianakas, A.E.; Papadaki, M.; Bikiaris, D.; Lambropoulou, D.A. Photocatalytical removal of fluorouracil using TiO_2-P25 and N/S doped TiO_2 catalysts: A kinetic and mechanistic study. *Sci. Total Environ.* **2017**, *578*, 257–267. [CrossRef]
13. Xue, Y.; Song, J.; Zhang, Y.; Kong, F.; Wen, M.; Zhang, G. Nitrate pollution and preliminary source identification of surface water in a semi-arid river basin, using isotopic and hydrochemical approaches. *Water* **2016**, *8*, 328. [CrossRef]
14. Kato, H.; Kudo, A. Photocatalytic reduction of nitrate ions over tantalate photocatalysts. *Phys. Chem. Chem. Phys.* **2002**, *4*, 2833–2838. [CrossRef]
15. Kotesh, K.M.; Bhavani, K.; Naresh, G.; Srinivas, B.; Venugopal, A. Plasmonic resonance nature of Ag-Cu/TiO_2 photocatalyst under solar and artificial light: Synthesis, characterization and evaluation of H_2O splitting activity. *Appl. Catal. B* **2016**, *199*, 282–291.
16. Xuming, Z.; Yu, L.C.; Ru-Shi, L.; Din, P.T. Plasmonic photocatalysis. *Rep. Prog. Phys.* **2013**, *76*, 046401–046407.
17. Stuart, H.R.; Hall, D.G. Island size effects in nanoparticle-enhanced photodetectors. *Appl. Phys. Lett.* **1998**, *73*, 3815–3817. [CrossRef]
18. Yang, T.; Tetsu, T. Plasmon-induced photoelectrochemistry at metal nanoparticles supported on nanoporous TiO_2. *Chem. Commun.* **2004**, *16*, 1810–1811.

19.   Syed, M.; Gerardo, H.; Daniel, M.; Joun, L.; Martin, M. Plasmonic photosensitization of a wide band gap semiconductor: Converting plasmons to charge carriers. *Nano Lett.* **2011**, *11*, 5548–5552.

20.   Nirmala, C.; Prashant, V.K. Improving the photoelectrochemical performance of nanostructured TiO_2 Films by Adsorption of gold nanoparticles. *J. Phys. Chem. B* **2000**, *104*, 10851–10857.

21.   Azusa, T.; Prashant, V.K. Capture, store, and discharge. Shuttling photogenerated electrons across TiO_2–silver interface. *ACS Nano.* **2011**, *5*, 7369–7376.

22.   Jian, L.; Fuyi, C. Plasmon enhanced photoelectrochemical activity of Ag-Cu nanoparticles on TiO_2/Ti substrates. *Int. J. Electrochem. Sci.* **2012**, *7*, 9560–9572.

23.   Jhuang, Y.Y.; Cheng, W.T. Fabrication and characterization of silver/titanium dioxide composite nanoparticles in ethylene glycol with alkaline solution through sonochemical process. *Ultrason. Sonochem.* **2016**, *28*, 327–333. [CrossRef]

24.   Ning, S.; Ding, L.; Lin, Z.; Lin, Q.; Zhang, H.; Lin, H.; Long, J.; Wang, X. One-pot fabrication of Bi_3O_4Cl/BiOCl plate-on-plate heterojunction with enhanced visible-light photocatalytic activity. *Appl. Catal. B Environ.* **2016**, *185*, 203–212. [CrossRef]

25.   He, Z.; Shi, Y.; Gao, C.; Wen, L.; Chen, J.; Song, S. Fas-associated factor 1 plays a negative regulatory role in the antibacterial immunity of locusta migratoria. *J. Phys. Chem. C* **2013**, *22*, 389–398.

26.   Henrik, J.; Alexei, S.; Zheshen, L.; Erik, S. XPS and FTIR investigation of the surface properties of different prepared titania nano-powders. *Appl. Surf. Sci.* **2005**, *246*, 239–249.

27.   Lopez, T.; Cuevas, J.L.; Ilharco, L.; Ramírez, P.; Rodríguez-Reinoso, F.; Rodríguez-Castellón, E. XPS characterization and E. Coli DNA degradation using functionalized Cu/TiO_2 nanobiocatalysts. *Mol. Catal.* **2018**, *449*, 62–71. [CrossRef]

28.   Mallikarjuna, K.; Kim, H. Synthesis of shape and size-dependent CuAg bimetallic dumbbell structures for organic pollutant hydrogenation. *Phys. E Low-dimens. Syst. Nanostruct.* **2018**, *102*, 44–49. [CrossRef]

29.   Méndezmedrano, M.G.; Kowalska, E.; Lehoux, A.; Herissan, A.; Ohtani, B.; Bahena, D.; Briois, V.; Colbeaujustin, C.; Rodríguezlópez, J.L.; Remita, H. Surface modification of TiO_2 with Ag nanoparticles and CuO nanoclusters for application in photocatalysis. *J. Phys. Chem. C* **2016**, *120*, 5143–5154.

30.   He, Y.; Zhu, Y.; Wu, N. Synthesis of nanosized $NaTaO_3$ in low temperature and its photocatalytic performance. *J. Solid State Chem.* **2004**, *177*, 3868–3872. [CrossRef]